ELSEVIER

Journal of Fluids and Structures 25 (2009) 1318–1333

JOURNAL OF FLUIDS AND STRUCTURES

www.elsevier.com/locate/jfs

Large-scale structures of turbulent flows over an open cavity

Woong Kang, Hyung Jin Sung*

Department of Mechanical Engineering, Korea Advanced Institute of Science and Technology, 373-1 Guseong-dong, Yuseong-gu, Daejeon 305-701, Korea

Received 30 November 2008; accepted 11 June 2009
Available online 19 August 2009

Abstract

Low Mach number turbulent flows over an open cavity were studied to investigate the quantitative characteristics of large-scale vortical structures responsible for self-sustained oscillations. Wind tunnel experiments with particle image velocimetry (PIV) were conducted in the range of the ratio of cavity length (L) to depth (D), $1<L/D<4$, when the incoming boundary layer is turbulent at $\mathrm{Re}_\theta = 830$ and 1810. Self-sustained oscillation modes were classified by varying the conditions of L/D and Re_θ. The oscillation modes were consistent with the number of vortical structures existing between the leading and trailing edges of the cavity. Proper orthogonal decomposition (POD) was employed to the spatial distributions of vertical velocity correlations on the lip line of cavity geometry. By examining the conditionally averaged distributions of the correlation coefficients of POD, the spatial characteristics of large-scale vortical structures for self-sustained oscillations were examined.

Keywords: Self-sustained oscillations; Large-scale vortical structure; Particle image velocimetry; Proper orthogonal decomposition

1. Introduction

Flows over an open cavity have received much attention due to the occurrence of self-sustained oscillations of velocity and pressure, which may induce acoustic noise or strong vibrations in engineering applications such as air and ground transportation. Thus, many numerical and experimental studies have been made over several decades to understand the mechanism underlying self-sustained oscillations and prevent undesired problems. The nature of oscillating behavior with a separated shear layer over an open cavity is known to be influenced by several flow parameters, which are the ratio of cavity length (L) to depth (D), Mach number (Ma), Reynolds number (Re) and the state of the incoming boundary layer.

In cavity flows with high Mach numbers, self-sustained oscillations over an open cavity originate from shear layer instabilities and acoustic feedback (Rossiter, 1964; Ahuja and Mendoza, 1995). In laminar flows with low Mach numbers, the mechanism of self-sustained oscillations was characterized by identifying the oscillation modes which are denoted by shear layer and wake modes (Gharib and Roshko, 1987). These oscillation modes were generated by hydrodynamic instabilities within the shear layers of laminar cavity flows (Rockwell and Naudascher, 1979; Rockwell and Kinsley, 1980; Howe, 1997; Yao et al., 2004). However, in turbulent cavity flows with low Mach number, it is not

*Corresponding author. Tel.: +82 42 350 3027; fax: +82 42 350 5027.
E-mail address: hjsung@kaist.ac.kr (H.J. Sung).

0889-9746/$ - see front matter © 2009 Elsevier Ltd. All rights reserved.
doi:10.1016/j.jfluidstructs.2009.06.005

Nomenclature

a_m	time-varying coefficient of mth mode
f	frequency of self-sustained oscillations (Hz)
q	stochastic data
D	cavity depth (mm)
K	kernel function
L	cavity length (mm)
M	total number of eigenmodes or snapshots
N	number of self-sustained oscillation modes
Re_D	Reynolds number, $U_\infty D/\nu$
Re_θ	Reynolds number, $U_\infty \theta/\nu$
R_{vv}	v–v two-point correlation coefficient
St_L	Strouhal number based on the length of the cavity
U_c	convection velocity (m/s)
U_∞	free-stream velocity (m/s)
v_{rms}	root mean square of vertical velocity (m/s)
x_0	streamwise position of reference point (mm)
y_0	vertical position of reference point (mm)
α_m	mth threshold of time-varying coefficient
δ	boundary layer thickness (mm)
δ_ω	vorticity thickness (mm)
θ	momentum thickness of incoming boundary layer (mm)
λ_{ci}	swirling strength
$\lambda_{\omega x}$	streamwise wavelength of vortical structure (mm)
σ_m	mth eigenmode
ψ_m	mth eigenvector
Ω	physical domain of stochastic data

clear to elucidate the occurrence of self-sustained oscillations due to the inherent fluctuations originated from turbulence (Grace et al., 2004; Chang et al., 2006).

Recently several attempts have been made to identify self-sustained oscillations of turbulent cavity flows by examining large-scale structures within the separated shear layer of the cavity (Oshkai et al., 2005; Geveci et al., 2003). Lin and Rockwell (2001) observed large-scale structures related to self-sustained oscillations with periodic pressure fluctuations in turbulent cavity flow. Ashcroft and Zhang (2005) also observed large-scale vortical structures, by examination of the instantaneous velocity fields and the statistical analysis of vertical velocity correlation, as evidence of self-sustained oscillations. Lee et al. (2008) showed that the spectral characteristics of large-scale structures are identical with the energy spectra of pressure fluctuations corresponding to the self-sustained oscillations by large eddy simulations. They identified large-scale structures responsible for self-sustained oscillations by employing proper orthogonal decompositions (POD) to the distributions of pressure fluctuations. More recently, Kang et al. (2008) demonstrated that self-sustained oscillation modes are determined by analyzing the distributions of vertical velocity, which reflect the organized nature of large-scale vortical structures.

Although previous studies found that the formation of large-scale vortical structures is essential for self-sustained oscillations, the main focus was limited mainly to ascertain the existence of self-sustained oscillations for few cases of cavity geometries. To understand the mechanism of self-sustained oscillations in turbulent cavity flows, it is indispensable to test in a wide range of parameters such as the length of the cavity (L/θ), Reynolds number (Re_θ) and ratio of length to depth (L/D), which could affect the occurrence of self-sustained oscillations. Moreover, quantitative analysis is needed to identify the spatial characteristics of large-scale vortical structures with regard to self-sustained oscillations.

The objective of the present study is to investigate the quantitative characteristics of large-scale vortical structures responsible for self-sustained oscillations with various turbulent cavity flows. To achieve this, we carried out particle image velocimetry (PIV) measurements in a range of $1<L/D<4$ when the incoming boundary layer is turbulent at $\mathrm{Re}_\theta = 830$ and 1810. Statistical analysis over the instantaneous PIV data was used to identify the oscillation modes with regard to large-scale structures. In addition, to elucidate the spatial characteristics of large-scale vortical structures, proper orthogonal decomposition (POD) was utilized to the velocity fluctuations within the separated shear layer, which was based on the spatial correlation of vertical velocity on the lip line of the cavity. Furthermore, conditional averaging with the correlation coefficients of POD was employed to represent the large-scale structures of the flows over an open cavity.

2. Experimental apparatus and procedure

Experiments were performed in a subsonic open-circuit wind tunnel. Details regarding the experimental apparatus are described in Kang et al. (2008). However, test sections were modified and extended for the present experiments. The cavity dimensions were 10–100 mm (length) × 10 or 25 mm (depth) × 630 mm (width). The length of the cavity was

designed to be adjustable while the depth of the cavity was fixed to 10 and 25 mm, in order to investigate the effect of length (L) to depth (D) ratios such as $L/D = 1$, 2 and 4 (see Fig. 1). In the present experiments, the inlet velocities were 6.85 and 14 m/s. The Reynolds numbers Re_θ defined based on the momentum thickness at these velocities were 830 and 1810, respectively. The boundary layer thickness (δ) and momentum thickness (θ) of the inlet boundary layer at $x/D = -4$ were 21, 19 and 1.77, 1.73 mm, respectively. Details of the flow parameters in the present study are given in Table 1.

Particle image velocimetry (PIV) techniques were employed to measure instantaneous velocity field of the cavity, as shown in Fig. 1. A laser light sheet was produced by a double-pulsed Nd:YAG laser (New Wave Research) that delivered 200 mJ of energy per pulse at 532 nm. The laser sheet illumination was collimated by a cylindrical lens before entering the test-section. Tracer particles in the flow fields were seeded by laskin nozzle submerged in an olive oil chamber. Particle images were captured by an 85 mm lens (Nikon, Micro) and a 12-bit CCD camera (Sensicam faster shutter, PCO Inc.) with 1280×1024 pixels. A field of view was changed from 30 mm × 24 mm to 112 mm × 90 mm in accordance with different geometries of the cavity. For each geometry and inlet velocity, 5000 instantaneous PIV images were acquired. An iterative algorithm with window offset and multiplication of two adjacent correlation planes were used to cross-correlate pairs of consecutive image maps (Hart, 2000). The final interrogation window size

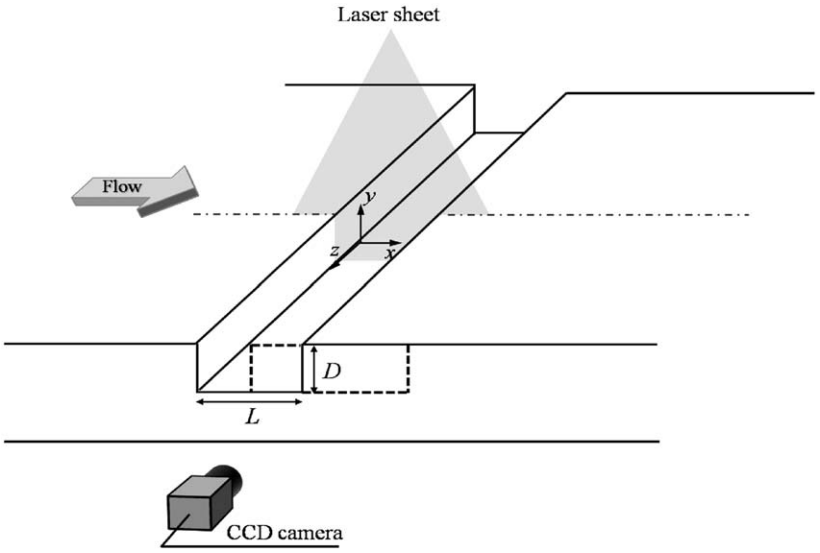

Fig. 1. Schematic diagram of cavity configuration.

Table 1
Experimental conditions.

L/D	D/θ	Re_θ	Ma
1	5.7	830	0.02
1	14	830	0.02
1	5.8	1810	0.04
1	15	1810	0.04
2	5.7	830	0.02
2	14	830	0.02
2	5.8	1810	0.04
2	15	1810	0.04
4	5.7	830	0.02
4	14	830	0.02
4	5.8	1810	0.04
4	15	1810	0.04

was 16×16 pixels with a 50% overlap. Particle displacements and turbulent quantities were computed using in-house PIV software. Velocity measurements for inflow parameter, e.g. velocity, boundary layer thickness and momentum thickness were obtained using a constant-temperature anemometer (IFA 300) and a single wire (TSI 1260). To resolve streamwise velocities, a total of 409,600 time-series data were acquired with a 7.5 kHz sampling rate and analyzed using LabVIEW software and an A/D board (NI 6052E, National Instrument Inc., USA).

3. Results and discussion

3.1. Time-mean and instantaneous velocity fields

PIV measurements were carried out at a total of 12 cases which include two different inlet velocities, two different depths and three ratios of length to depth, as listed in Table 1. For all configurations studied, the time-mean flow fields were characterized by the open cavity type, which exhibits the impingement of the separated shear layer and large recirculation flow. Fig. 2 shows time-averaged streamlines and contours of streamwise velocity for $L/D = 1$, 2 and 4 with $\mathrm{Re}_\theta = 1810$ and $D/\theta = 5.8$. In all three figures, a clockwise rotating vortex is observed within the cavity. A counterclockwise rotating vortex in the upstream region inside the cavity is induced by the clockwise rotating vortex for $L/D = 2$ and 4, whereas a clockwise rotating vortex fills the whole cavity for $L/D = 1$.

To investigate the characteristics of the separated shear layer in the open cavity, the growth rate of the separated shear layer between the leading and trailing edges was quantified using vorticity thickness (δ_ω). As a measure of the shear layer thickness, the vorticity thickness was employed to time-averaged flow fields, which is defined as

$$\delta_\omega = \frac{U_2 - U_1}{\partial U/\partial y|_{\max}}, \tag{1}$$

where U_2 and U_1 are the speeds of the upper and lower streams, respectively (Brown and Roshko, 1974). In the present study, U_2 is the free-stream velocity (U_∞) and $U_1 = 0$. Fig. 3 shows the variation of the vorticity thickness along the lip line of the cavity geometry, where the lip line is a straight line from the leading edge to the trailing edge. The vorticity thickness (δ_ω) is normalized by the cavity depth. The rate of growth ($\mathrm{d}\delta_x/\mathrm{d}x$) for each system of $L/D = 1$, 2 and 4 shows the same trend, which is a linear growth until the separated shear layer encounters the trailing edge and thereafter a sharp decay in Fig. 3(a). Even though the incoming flow and the depth of the cavity are different, the spreading rates are similar as shown in Fig. 3(b).

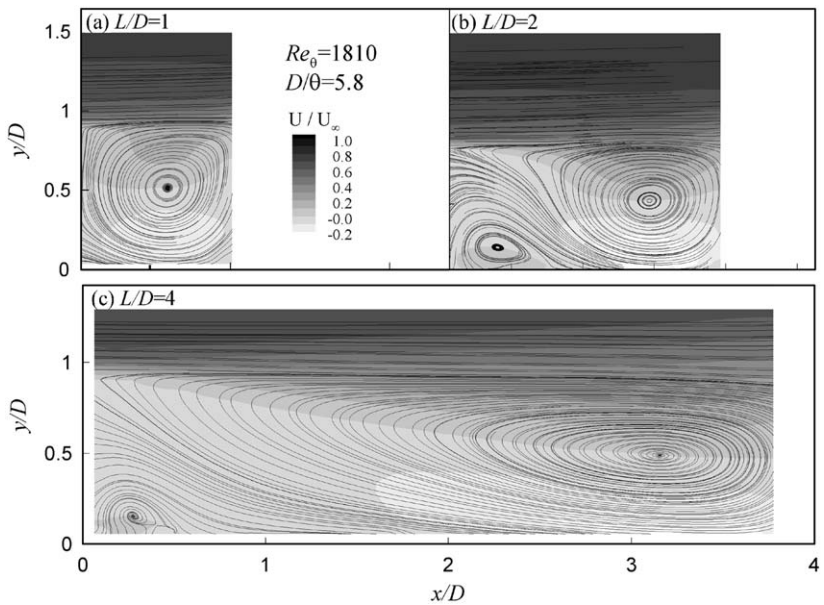

Fig. 2. Mean velocity and streamline for $\mathrm{Re}_\theta = 1810$, $D/\theta = 5.8$: (a) $L/D = 1$; (b) $L/D = 2$ and (c) $L/D = 4$.

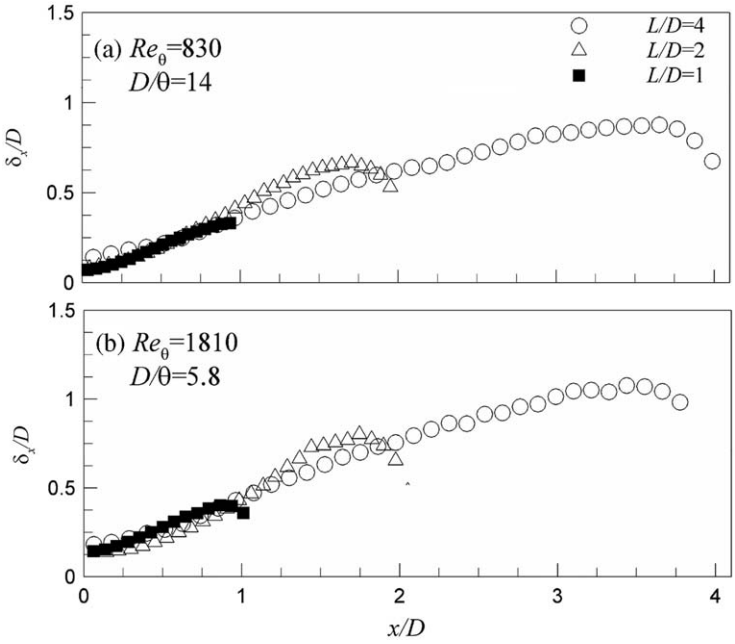

Fig. 3. Vorticity thickness along the shear layer for $L/D = 1$, 2 and 4: (a) $\mathrm{Re}_\theta = 830$ and $D/\theta = 14$ and (b) $\mathrm{Re}_\theta = 1810$ and $D/\theta = 5.8$.

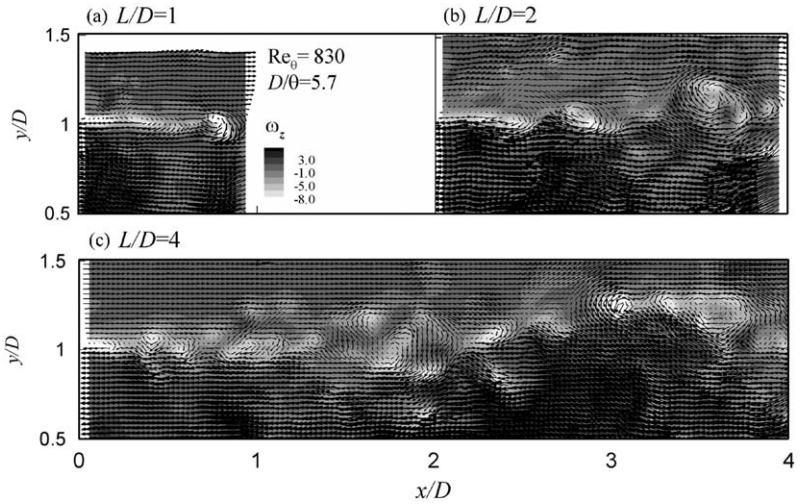

Fig. 4. Instantaneous velocity field by Galilean decomposition for $\mathrm{Re}_\theta = 830$ and $D/\theta = 5.7$: (a) $L/D = 1$, (b) $L/D = 2$ and (c) $L/D = 4$.

Next, we consider the large-scale vortical structures regarding the growth of the separated shear layer over the open cavity. Fig. 4 shows a vector field of instantaneous velocity and contours of vorticity for $L/D = 1$, 2 and 4. To more clearly observe the large-scale vertical structure, Galilean decomposition is applied with a convective velocity of $0.55U_\infty$, as used in previous studies (Sarohia, 1977; Ahuja and Mendoza, 1995; Larchevêque et al., 2003; Kang et al., 2008). When the convective velocity is subtracted from the instantaneous velocity, several vortical structures are observed between the leading and trailing edges in the three figures. In all configurations, the length scale of vortical structure within the separated shear layer grows with it moves downstream. Note that the large-scale vortical structures in Fig. 4 are similar to the vortical characteristics of self-sustained oscillations obtained in previous studies (Gharib and Roshko, 1987; Lin and Rockwell, 2001; Kang et al., 2008).

3.2. Self-sustained oscillation modes in the cavity flow

To further elucidate the characteristics of large-scale vortical structures, we examine two-point spatial correlation coefficients of vertical velocity fluctuations (Fig. 5). This is defined as

$$R_{vv}(x/D, y/D; x_0, y_0) = \frac{\langle v(x/D, y/D) v(x/D + x_0, y/D + y_0) \rangle}{v_{\mathrm{rms}}(x/D, y/D) v_{\mathrm{rms}}(x/D + x_0, y/D + y_0)}, \tag{2}$$

where (x_0, y_0) represents a reference point. Here, $\langle\ \rangle$ denotes an ensemble average of 5000 PIV images. These reference points are located at $(x/D,\ y/D) = (1, 1)$, (2, 1) and (3, 1) as shown in Fig. 5. Alternating patterns of positive and negative coefficients are observed for all cases. As reported by Little et al. (2007) and Kang et al. (2008), the alternating pattern represents the formation of large-scale vortical structures within the separated shear layer. On moving downstream, the length scale of the alternating pattern increases. This is consistent with the growth of vortical structure within the shear layer as shown in Fig. 4.

To quantify the growth of large-scale vortical structures, the streamwise wavelength of the vortical structure is defined as the distance between consecutive negative peaks of the v–v correlation coefficient along the lip line of the cavity geometry (Kang et al., 2008), as shown in the inset of Fig. 6(b). As the reference point moves downstream, the wavelength gradually increases from $0.5D$ near the leading edge to $2D$ near the trailing edge, as shown in Fig. 6(a). The streamwise averaged wavelength is calculated as $\lambda_{x,\ \mathrm{avg}}/D = 1.37$ within the cavity length, as indicated by dashed lines. Gharib and Roshko (1987) determined the Nth oscillating mode of incompressible flows over an open cavity by using Rossiter's empirical equation

$$\frac{L}{\lambda_x} = \frac{fL}{U_{c,\mathrm{avg}}} = N, \tag{3}$$

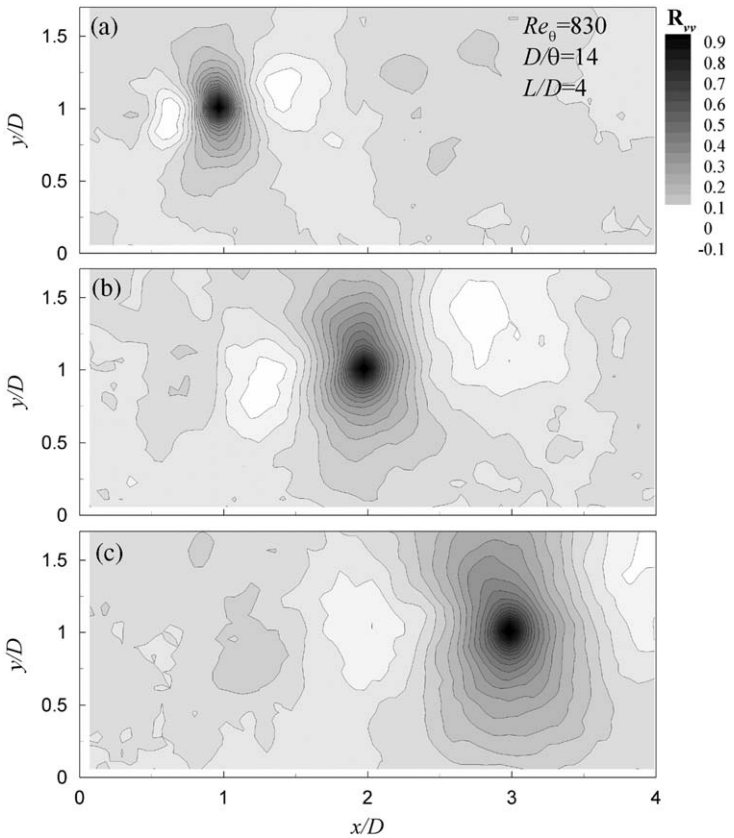

Fig. 5. Two-point spatial correlation for $\mathrm{Re}_\theta = 830$, $D/\theta = 14$ and $L/D = 4$: (a) $x/D = 1$ and $y/D = 1$, (b) $x/D = 2$ and $y/D = 1$ and (c) $x/D = 3$ and $y/D = 1$.

where f is the oscillating frequency and $U_{c,\mathrm{avg}}$ is the averaged convection velocity. The closest integer of N in the Nth mode of oscillation is the number of vortical structures existing between the leading and trailing edges. When the incoming flow over a cavity is turbulent with very low Mach number, Eq. (3) is also available because the acoustic

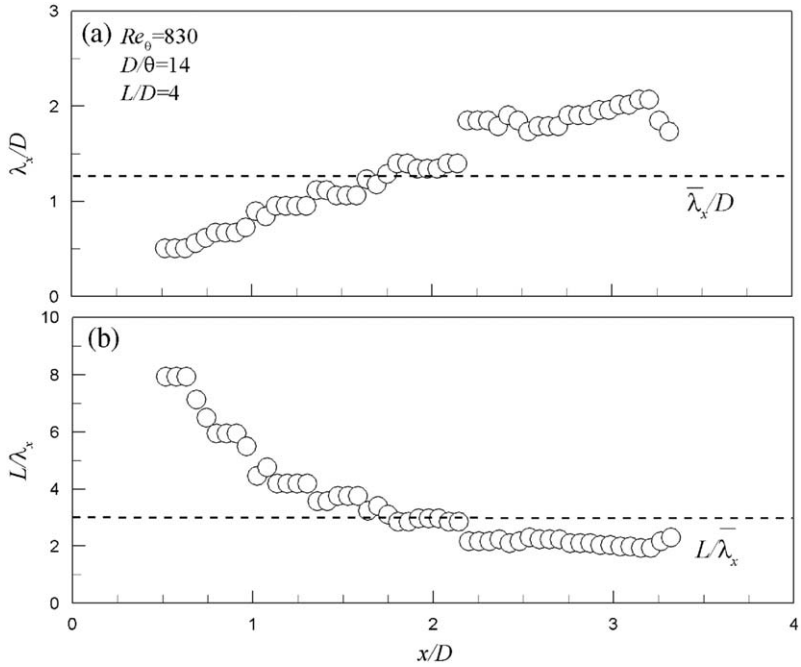

Fig. 6. Wavelengths of two-point correlation along the lip line of cavity geometry for $\mathrm{Re}_\theta = 830$, $D/\theta = 14$ and $L/D = 4$: (a) the distribution of λ_x/D and (b) the distribution of L/λ_x.

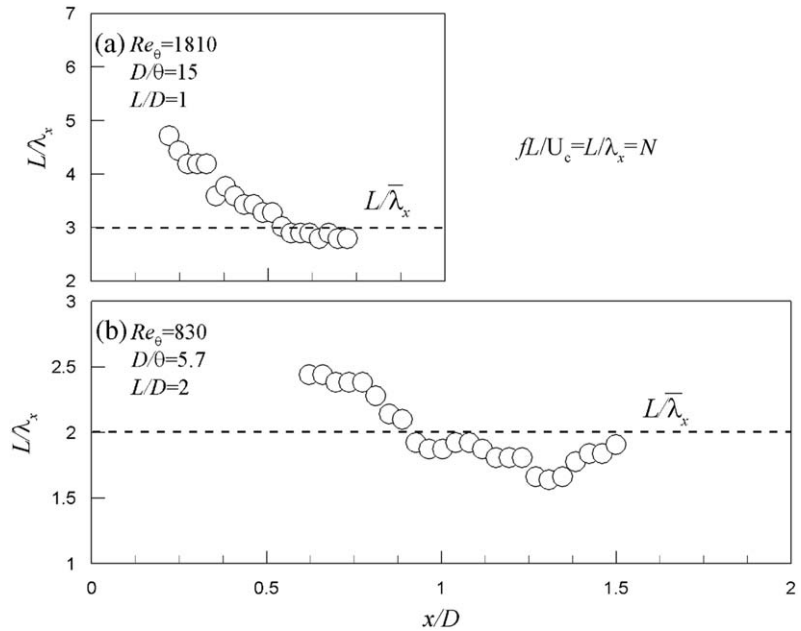

Fig. 7. Wavelengths of two-point correlation along the lip line of cavity geometry: (a) the distribution of L/λ_x for $\mathrm{Re}_\theta = 1810$, $D/\theta = 15$ and $L/D = 1$ and (b) the distribution of L/λ_x for $\mathrm{Re}_\theta = 830$, $D/\theta = 5.7$ and $L/D = 2$.

wavelength (λ) is much longer than the cavity length. Therefore, Kang et al. (2008) identified the Nth mode of self-sustained oscillations based on the the streamwise averaged wavelength $\lambda_{x,\mathrm{avg}}$ and cavity length L. Fig. 6(b) represents distributions of the cavity length over streamwise averaged wavelengths L/λ_x on the lip line of the cavity, which can be expressed as Eq. (3). The decrease of L/λ_x along the lip line of the cavity is similar to the trend observed previously in dominant oscillation frequency distribution of the flow over a backward-facing step. This means that the small vortices are generated near the leading edge of the cavity and grow into a large-scale vortical structure as it convects downstream until the trailing edge. The streamwise averaged wavelength $L/\lambda_{x,\mathrm{avg}}$ is calculated as 2.9 within the cavity length, as indicated by dashed line in Fig. 6(b). By Eq. (3), this value is very close the integer 3, which can be regarded as the number oscillation modes and vortical structures within the open cavity. This result is consistent with the numbers of vortical structures observed in the instantaneous velocity fields.

Fig. 7 shows the distributions of L/λ_x on the lip line of the cavity with different geometries such as $L/D = 1$ and 2. They represent the decrease of L/λ_x along the separated shear layer of the cavity. The averaged wavelengths $L/\lambda_{x,\mathrm{avg}}$ are calculated as 2.9 for $L/D = 1$ and 1.9 for $L/D = 2$. These values, which can be regarded as the closest integer 3 and 2, are also consistent with the number of large-scale vortical structures observed in the instantaneous velocity fields. Different numbers of large-scale vortical structures are obtained in the various cavity flows of the present configuration. This means that there are many oscillation modes depending on the inflow parameters and cavity geometries.

By examining the afore-stated streamwise averaged wavelength, the oscillation modes of each system can be classified. Fig. 8 represents the oscillation modes, which occur at different cavity lengths (L/θ) and inflow velocities (Re_θ). Mode 1, mode 2 and mode 3 are denoted by a circle, a triangle and a square, respectively, while non-oscillation is represented by cross. When $\mathrm{Re}_\theta = 1810$, the first oscillation mode appears in the shortest cavity, i.e., $L/\theta = 5.8$ and $L/D = 1$. When $L/\theta = 11.6$ and $L/D = 2$, the second oscillation mode occurs. As the length of the cavity increases beyond $L/\theta = 15$, flows begin to oscillate in the third mode, which remains unchanged although the cavity length increases further in the present study. Meanwhile, in the low Reynolds number, i.e., $\mathrm{Re}_\theta = 830$, the third oscillation mode starts to appear in the cavity with a longer length than that at $\mathrm{Re}_\theta = 1810$. The second mode also appears at a longer cavity length. The higher oscillation modes may occur as Re_θ and L/θ increase further. In addition, note that no self-sustained oscillations occur at $L/\theta = 5.7$ and $\mathrm{Re}_\theta = 830$. To clarify the non-oscillation case, two-point spatial correlation is obtained as discussed in Fig. 5. Fig. 9(a) represents two-point spatial correlation coefficients of vertical velocity fluctuations when the reference point is set at $(x/D, y/D) = (0.5, 1)$. Different from the results of other cases, the alternating patterns of positive and negative coefficients are not observed between the leading and trailing edges of the cavity. This means that there are no formations of large-scale vortical structures in the cavity. These features can be ascertained in the distribution of v–v correlation coefficients along the lip line of the cavity. As shown in Fig. 9(b), the v–v correlation coefficients have positive values between the leading and trailing edges of the cavity.

3.3. Proper orthogonal decomposition analysis

The proper orthogonal decomposition (POD) introduced by Lumley (1967) is designed to find an orthogonal basis set from an ensemble of stochastic data $q(\vec{x}, t)$ which can be a significant quantity in the large structures of flow fields. A set of basis functions is determined to maximize the value of mean-square projection on stochastic data, which becomes the most similar to the original ensemble of data. Consequently, this amounts to solving an eigenvalue problem for finding the largest eigenvalue

$$\int_\Omega K(\vec{x}, \vec{r})\psi_m(\vec{r})d\vec{r} = \lambda_m\psi_m(\vec{x}), \tag{4}$$

where $\psi_m(\vec{x})$ and λ_m is a set of basis functions, i.e., eigenvector and eigenvalue. The kernel $K(\vec{x}, \vec{r})$ is a two-point spatial correlation tensor, which is defined as

$$\vec{x}, \vec{r}) = \langle q(\vec{x})q(\vec{x} + \vec{r})\rangle. \tag{5}$$

The stochastic data $q(\vec{x}, t)$ can be reconstructed in the linear combination of orthogonal basis functions

$$q(\vec{x}, t) = \sum_{m=1}^{M} \mu_m\varphi_m(t)\psi_m(\vec{x}), \tag{6}$$

where ϕ_m are time-varying coefficients. In the linear combination, each basis function is scaled by μ_m.

In the previous studies (Lumley, 1967; Liu et al., 2001; Kostas et al., 2002), the kernel function of POD is determined to find the orthogonal eigenmodes of velocity fluctuations which were chosen for significant quantities of large-scale structures in the flow. The kernel functions, i.e., correlation tensors of velocity fluctuations, correspond to total kinetic

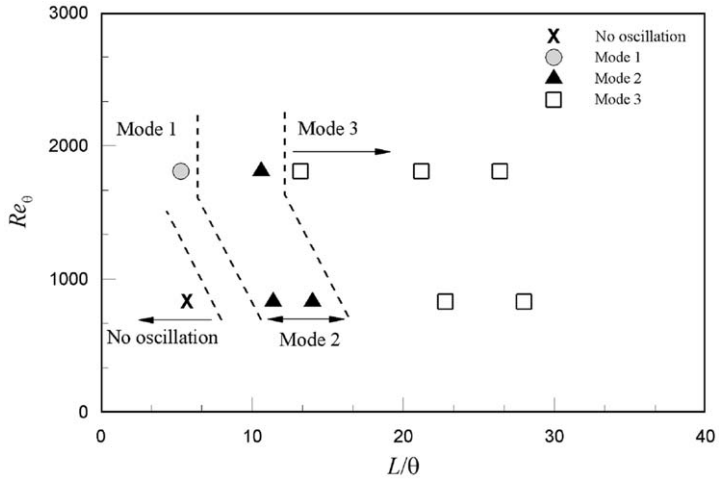

Fig. 8. Oscillation modes for Re_θ and L/θ.

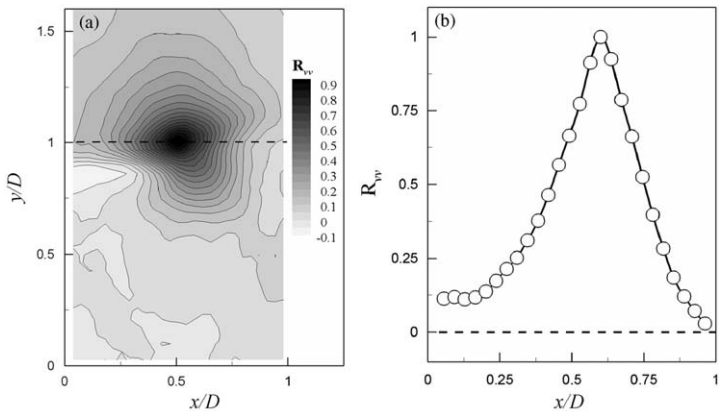

Fig. 9. Two-point spatial correlation for $\mathrm{Re}_\theta = 830$, $D/\theta = 5.7$ and $L/D = 1$.

energy. However, the total kinetic energy is not an effective criterion for disclosing the self-sustained oscillation modes in turbulent cavity flows with low Mach number, due to the presence of inherent fluctuations originated from turbulence and the weak coherence of large-scale vortical structures in the absence of acoustic resonance. Meanwhile, the oscillating behaviors of the large-scale vortical structures are well extracted by the two-point spatial correlations of vertical velocity fluctuations along the lip line of the cavity, as mentioned in Section 3.2. Hence, in the present study, the vertical velocity fluctuations along the lip line are chosen for use in the application of POD analysis. The vertical velocity fluctuations can be expressed as a linear combination of a set of basis functions as follows:

$$v(x,t) = \sum_{m=1}^{M} \mu_m \varphi_m(t) \sigma_m(x), \tag{7}$$

where $\sigma_m(x)$ represents the mth eigenmode; 5000 instantaneous velocity fluctuations of the cavity flows are used for the present POD analysis.

Fig. 10 shows the first four eigenmodes of the vertical velocity fluctuations along the lip line for $\mathrm{Re}_\theta = 830$, $D/\theta = 14$ and $L/D = 1$. The periodic distributions are observed in the first and second modes in Fig. 10(a), which are related to the oscillating behavior of the separated shear layer. Kang et al. (2008) suggested necessary conditions for identifying the large-scale vortical structures in the cavity flow, which contain the change of vertical velocity from positive to negative value on the lip line of the cavity. Through applying the same procedure of vortical structure identification to the eigenmode of vertical velocity, in the first and second eigenmodes, two large-scale vortical structures are detected

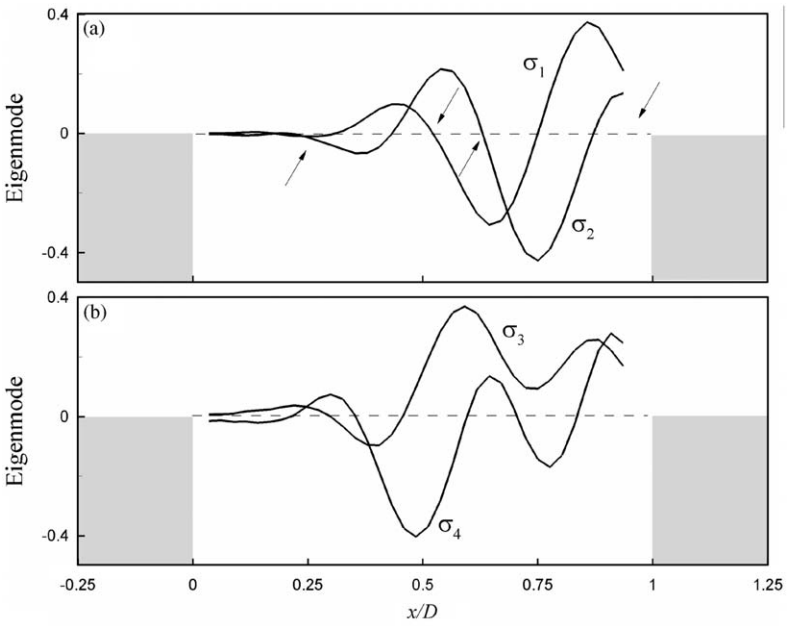

Fig. 10. Eigenmodes of POD for $\mathrm{Re}_\theta = 830$, $D/\theta = 14$ and $L/D = 1$: (a) modes 1 and 2 and (b) modes 3 and 4.

between the leading and trailing edges, respectively, as denoted by arrows. It is consistent with the self-sustained oscillation modes corresponding to $N = 2$, which are determined by the streamwise averaged wavelength as discussed above. This means that the most energetic behaviors of the separated shear layer are the large-scale vortical structures responsible for self-sustained oscillations. When regarding the shapes of the first and second eigenmodes as a sinusoidal wave, the amplitude and period of the wave are observed to be increased going downstream. This result is relevant to the large-scale vortical structures between the leading and downstream edges with the growth of shear layer as observed previously. The first mode is very similar to the second mode with a phase shift as expected when the flow is experiencing a global mean advection. The phase difference is estimated to be a quarter of one period. On the contrary, irregular and high wavenumber motions of separated shear layer are observed in the third and fourth modes, as shown in Fig. 10(b). In addition, it is difficult to find evidence of regular vortical structures. In the previous studies of laminar flow, Podvin et al. (2006) showed that the oscillating behaviors of separated shear layer are observed in the first two modes, whereas the next higher modes are related to the recirculation of the primary vortex inside cavity.

Fig. 11 shows the energy contribution of each mode, which is represented by the level of eigenvalue with a circle symbol. The accumulation of eigenvalues at each mode is represented by a solid line, which is normalized by the total sum. The contributions of the first two eigenmodes are almost 40% of the total energy. Close values of the first two modes support that the two modes are originated from an identical motion of the large-scale vortical structures. The relationship of the two modes is clearly shown in the phase diagram of Fig. 12, where the horizontal and vertical axes represent the time-varying coefficients a_1 and a_2, respectively. The time-varying coefficient $a_m(t)$ of the mth eigenmode is calculated by

$$a_m(t) = \mu_m \phi_m(t) = \int_\Omega v(x,t)\sigma_m(x)\mathrm{d}x. \tag{8}$$

When the maximum value of time-varying coefficients a_m is found to be a_1 or a_2 in every instantaneous field, distributions of the first and second mode coefficients are plotted in Fig. 12. It is interesting to find that the coefficients a_1 and a_2 are more or less located around a circle. If the two signals oscillate with constant amplitude and the phase difference is a quarter of one period, a complete circle is expected to be drawn. For the present distribution of the coefficients a_1 and a_2, the scatter around a theoretical circle means that small fluctuations of oscillating amplitudes and nearly constant phase difference are expected in the first two eigenmodes.

Next, to elucidate the spatial characteristics of the cavity flow corresponding to the dominant eigenmodes, i.e., the first and second modes, we used the conditionally averaged distribution of the correlation coefficients which was used in Lee et al. (2008) with direct numerical simulations of turbulent flows over an open cavity. In Eq. (8), the variable $a_m(t)$

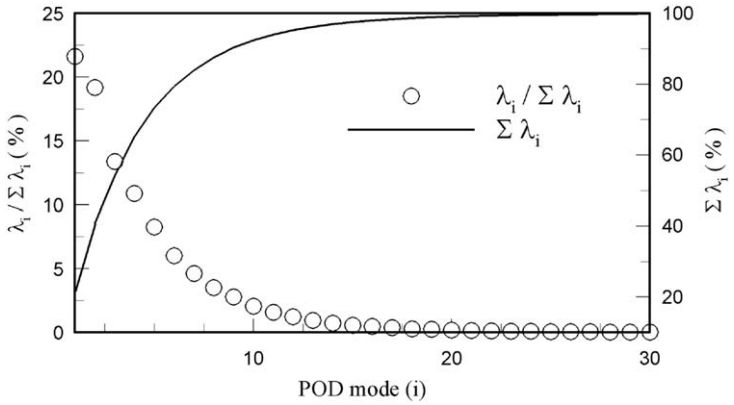

Fig. 11. Energy contribution of eigenvalues for $\mathrm{Re}_\theta = 830$, $D/\theta = 14$ and $L/D = 1$.

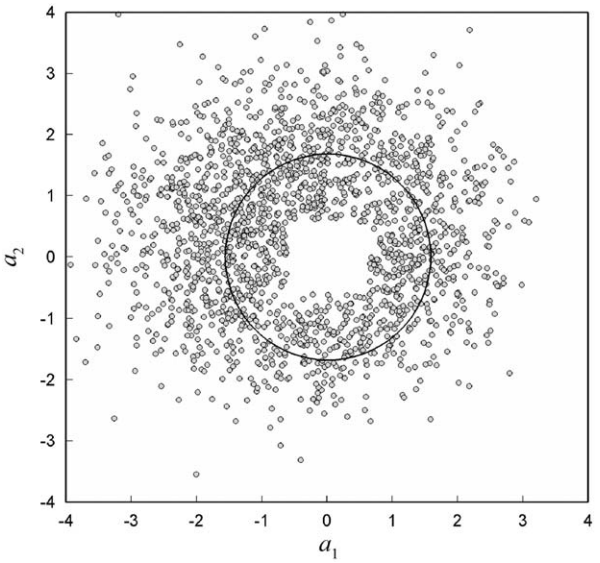

Fig. 12. Phase diagram of time-varying coefficients a_1 and a_2 for $\mathrm{Re}_\theta = 830$, $D/\theta = 14$ and $L/D = 1$.

can be regarded as an instantaneous correlation coefficient between instantaneous vertical velocity fluctuations $v(x, t)$ along the lip line and the mth eigenmode $\sigma_m(x)$. If the coefficient $a_m(t)$ is very large in the instantaneous velocity fields, the distribution of the instantaneous vertical velocity is very similar to the mth eigenmode. Thus, the conditional averaging of the instantaneous velocity field based on the correlation coefficient is estimated as

$$\langle \underline{u} | a_m(t) \geq \alpha_m \rangle = u_m(x), \tag{9}$$

where α_m is a threshold and we set $\alpha_m = 2(a_m)_{rms}$. Fig. 13 shows conditionally averaged distributions of the velocity fluctuations corresponding to the first two eigenmodes of vertical velocity fluctuations. The contour map is the distribution of swirling strength λ_{ci}, which is known to be an effective parameter for identifying vortical structures (Zhou et al., 1999). In Fig. 13(a), two large-scale vortical structures are observed at $x/D = 0.5$ and 0.95 with a clockwise rotation of the velocity vector coinciding with the local peaks of the λ_{ci} distribution. This is concurrent with the vortical structure detected in the first eigenmode distribution of the vertical velocity fluctuations in Fig. 10(a). In Fig. 13(b), we can observe two large-scale vortical structures with the peaks of λ_{ci} at $x/D = 0.25$ and 0.6, which may be the next phase of an identical motion. The position of the vortical structure is consistent with that of the second eigenmode. This consistency shows a successful estimation of velocity fields corresponding to the first two eigenmodes. The velocity fields corresponding to the first two eigenmodes represent the most energetic behaviors of the separated shear layer which are the large-scale vortical structures responsible for self-sustained oscillations. Through inspecting the conditionally

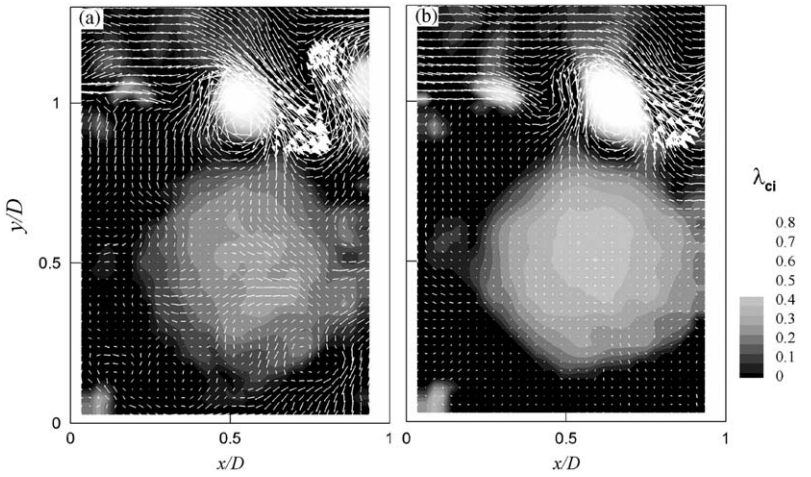

Fig. 13. Conditionally averaged distributions of velocity fluctuations for $Re_\theta = 830$, $D/\theta = 14$ and $L/D = 1$: (a) the first eigenmode and (b) the second eigenmode.

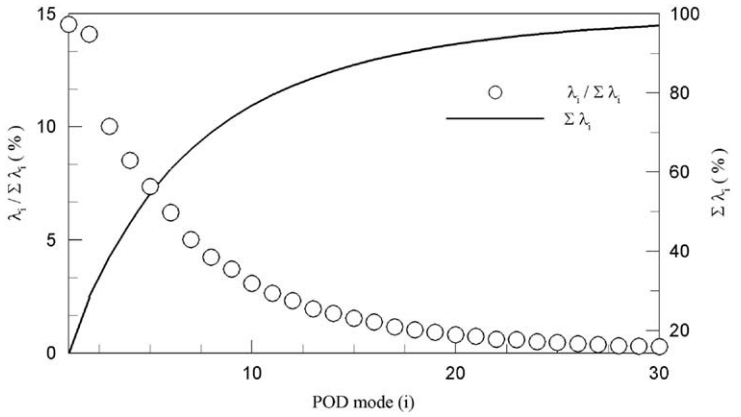

Fig. 14. Energy contribution of eigenvalues for $Re_\theta = 1810$, $D/\theta = 5.8$ and $L/D = 4$.

averaged velocity fields of the first two eigenmodes, we can understand the spatial characteristics of turbulent flow over an open cavity when the self-sustained oscillations take place. After the flow is separated near the leading edge, the formation of vortical structures starts to appear with the wave motions of velocity vectors. As the flow moves downstream, the length scale of the vortical structures gradually increases and the magnitude of velocity fluctuations becomes larger within the separated shear layer. Finally, the vortical structures are going to be ejected near the trailing edge.

Fig. 14 presents the energy contribution and local sum of eigenvalues for $Re_\theta = 830$, $D/\theta = 5.3$ and $L/D = 4$. The first and second eigenvalues are almost the same and contain a large portion (about 30%) of the total energy. Fig. 15 shows distributions of the time-varying coefficients for the first and second eigenmodes. The close values of eigenvalues and the circular shape of time-varying coefficients in the first two eigenmodes can be explained as identical structure motions with a phase difference, which are the most energetic structure in the separated shear layers.

Fig. 16 shows distributions of the first and second eigenmodes and conditional averaging velocity fluctuation fields corresponding to the two eigenmodes for $Re_\theta = 1810$, $D/\theta = 5.8$ and $L/D = 4$. In Fig. 16(a), as indicated by arrows, three large-scale vortical structures are detected in the first and second eigenmode distributions, respectively. They are also observed with clockwise rotations of the velocity vector coinciding with the local peaks of λ_{ci} in velocity fluctuations, which are determined by conditionally averaging under the criterion of correlation coefficient α_m, corresponding to the first two eigenmodes in Fig. 16(b) and (c). Moreover, this result is concurrent with self-sustained modes corresponding to $N = 3$, which are calculated by the streamwise averaged wavelength, as shown in Fig. 8. This

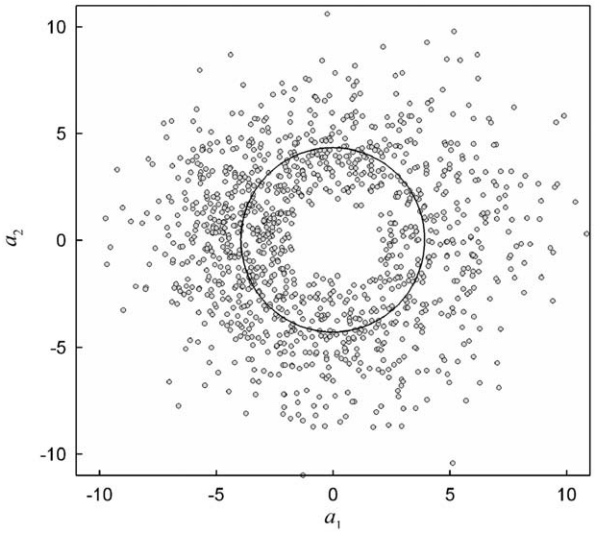

Fig. 15. Phase diagram of time-varying coefficients a_1 and a_2 for $\mathrm{Re}_\theta = 1810$, $D/\theta = 5.8$ and $L/D = 4$.

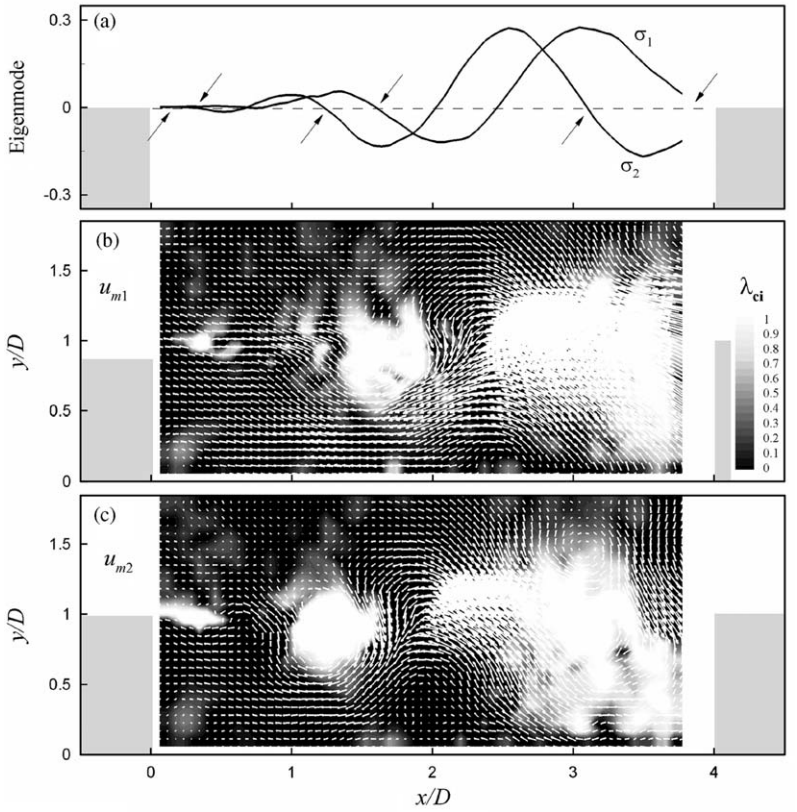

Fig. 16. Eigenmodes and conditionally averaged distributions of velocity fluctuations for $\mathrm{Re}_\theta = 1810$, $D/\theta = 5.8$ and $L/D = 4$.

consistency supports that the spatial characteristics of self-sustained oscillations are represented by the Nth large-scale vortical structures, which are the most dominant flow structures within the separated shear layer of the turbulent cavity flows.

Finally, we carry out a POD analysis for a system with $Re_\theta = 830$, $D/\theta = 5.7$ and $L/D = 1$, where no oscillation modes occur from the two-point spatial correlation of vertical velocity fluctuations, as shown in Fig. 9. Fig. 17(a) represents the energy contribution of eigenmodes and the accumulation of eigenvalues. Different from the results of other cases like Figs. 11 and 14, only the first eigenmode is dominant with about 35% contribution of the total energy. The contributions of other modes decrease for higher modes. Fig. 17(b) shows the distribution of the first and second eigenmodes of the vertical velocity fluctuations along the lip line. It is difficult to find evidence of large-scale vortical structure. In addition, the shapes of two eigenmodes are different from each other, which may have originated from different flow motions. Fig. 18 represents the conditionally averaged distributions of velocity fluctuations

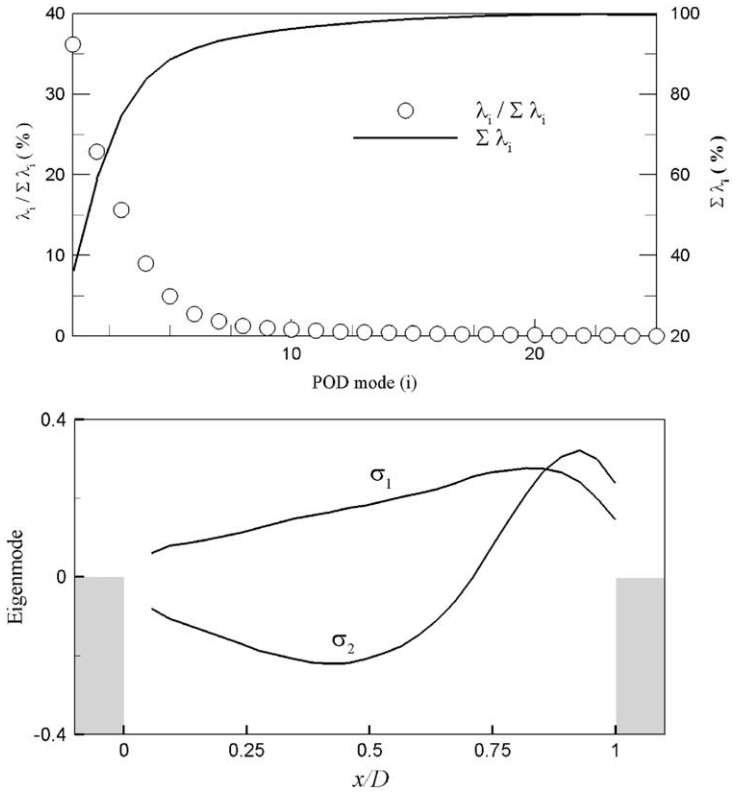

Fig. 17. Energy contribution of eigenvalues and eigenmodes for $Re_\theta = 830$, $D/\theta = 5.7$ and $L/D = 1$.

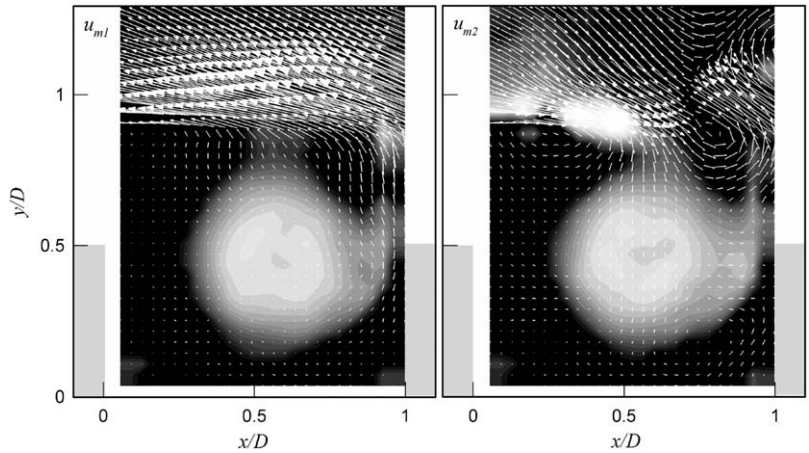

Fig. 18. Conditionally averaged distributions of velocity fluctuations for $Re_\theta = 830$, $D/\theta = 5.7$ and $L/D = 1$.

corresponding to the first and second modes. In Fig. 18(a), the pattern of velocity fluctuations by conditional averaging of the first eigenmode is similar to the mean flow distribution over an open cavity. Meanwhile, for the second eigenmode, the counterclockwise rotation of velocity vectors is observed between the leading and trailing edges. The core of rotation is not coincident with the local peak of λ_{ci}, which means that it is not a vortical structure.

4. Conclusions

We performed PIV measurements and POD analysis in turbulent flows over an open cavity to see the quantitative characteristics of the large-scale vortical structures responsible for self-sustained oscillations. Wind tunnel experiments were conducted in the range of $1<L/D<4$, when the incoming boundary layer is turbulent at $Re_\theta = 830$ and 1810. The growth rates of the separated shear layer thickness for $L/D = 1$, 2 and 4 showed a similar trend, i.e., a linear growth until the separated shear layer encounters the trailing edge and then a sharp decay. By examining the steamwise averaged wavelength of the vortical structures, the self-sustained oscillation modes were determined, which were consistent with the number of vortical structures existing between the leading and trailing edges of the cavity. When $Re_\theta = 1810$, the first oscillation mode appears for the system of $L/\theta = 5.8$ and $L/D = 1$. As the length of the cavity increases, the second and third oscillation modes occur at $L/\theta = 11.6$ and 15, respectively. For low Reynolds number ($Re_\theta = 830$), the second and third oscillation modes start to appear in the cavity with a longer length than that of $Re_\theta = 1810$, whereas no oscillations occur at $L/\theta = 5.7$. To elucidate the spatial characteristics of the large-scale vortical structures, POD analysis was applied to the spatial correlation of vertical velocity on the lip line of the cavity. The first and second eigenmodes of vertical velocity contain relatively large contributions of total energy. The two modes are originated from an identical structure motion of the separated shear layer with a phase shift. By applying the vortical structure identification to the first and second eigenmodes of vertical velocity, large-scale vortical structures are detected, which coincide with the self-sustained oscillation modes determined by the streamwise wavelength. By examining conditional averaging under the criterion of a strong correlation between the first two eigenmodes and the distribution of instantaneous vertical velocity, velocity fields corresponding to the self-sustained oscillations were obtained. Conditionally averaged velocity fluctuation fields showed the formation and development of large-scale vortical structures within the separated shear layer over an open cavity, which is responsible for self-sustained oscillations.

Acknowledgement

This work was supported by the Creative Research Initiatives of the Korea Science & Engineering Foundation.

References

Ahuja, K., Mendoza, J., 1995. Effects of cavity dimensions, boundary layer and temperature on cavity noise with emphasis on benchmark data to validate computational aeroacoustics codes. Final Report Contract NASA-19061, Task 13, NASA Contract Report.

Ashcroft, C., Zhang, X., 2005. Vortical structures over rectangular cavities at low speed. Physics of Fluids 17, 015104.

Brown, A., Roshko, A., 1974. On density effects and large structure in turbulent mixing layers. Journal of Fluid Mechanics 64, 775.

Chang, K.C., Constantinescu, G., Park, S.O., 2006. Analysis of the flow and mass transfer processes for the incompressible flow past an open cavity with a laminar and a fully turbulent incoming boundary layer. Journal of Fluid Mechanics 561, 113–145.

Geveci, M., Oshkai, P., Rockwell, D., Lin, J.-C., Pollack, M., 2003. Imaging of the self-excited oscillations of flow past a cavity during generation of a flow tone. Journal of Fluids and Structures 18, 665–694.

Gharib, M., Roshko, A., 1987. The effect of flow oscillations on cavity drag. Journal of Fluid Mechanics 177, 501–530.

Grace, S.M., Dewar, W.G., Wroblewski, D.E., 2004. Experimental investigation of the flow characteristics within a shallow wall cavity for both laminar and turbulent upstream boundary layers. Experiments in Fluids 36, 791–804.

Hart, D.P., 2000. PIV error correction. Experiments in Fluids 29, 13–22.

Howe, M.S., 1997. Low Strouhal number instabilities of flow over apertures and wall cavities. Journal of the Acoustical Society of America 102, 772–780.

Kang, W., Lee, S.B., Sung, H.J., 2008. Self-sustained oscillations of turbulent flows over an open cavity. Experiments in Fluids 45, 693–702.

Kostas, J., Soria, J., Chong, M.S., 2002. Particle image velocimetry measurements of a backward-facing step. Experiments in Fluids 33, 838–853.

Larchevêque, L., Sagaut, P., Mary, I., Labbé, O., 2003. Large-eddy simulation of a compressible flow past a deep cavity. Physics of Fluids 15, 193–210.

Lee, S.B., Kang, W., Sung, H.J., 2008. Organized self-sustained oscillations of turbulent flows over an open cavity. AIAA Journal 46, 278–296.

Lin, J.-C., Rockwell, D., 2001. Organized oscillations of initially turbulent flow past a cavity. AIAA Journal 39, 1139–1151.

Little, J., Debiasi, M., Caraballo, E., Samimy, M., 2007. Effects of open-loop and closed-loop on subsonic cavity flows. Physics of Fluids 19, 065104.

Liu, Z., Adrian, R.J., Hanratty, T.J., 2001. Large-scale modes of turbulent channel flow: transport and structure. Journal of Fluid Mechanics 448, 53–80.

Lumley, J.L., 1967. The structure of inhomogeneous turbulence. In: Yaglom, A.M., Tatarsky, V.I. (Eds.), Atmosphere Turbulence and Wave Propagation. Nauka, Moscow, pp. 166–178.

Oshkai, P., Geveci, M., Rockwell, D., Pollack, M., 2005. Imaging of acoustically coupled oscillations due to flow past a shallow cavity: effect of cavity length scale. Journal of Fluids and Structures 20, 277–308.

Podvin, B., Fraigneau, Y., Lusseyran, F., Gougat, P., 2006. A reconstruction method for the flow past an open cavity. ASME Journal of Fluids Engineering 128, 531–540.

Rockwell, D., Kinsley, C., 1980. Observation of the three-dimensional nature of unstable flow past a cavity. Physics of Fluids 23, 425–431.

Rockwell, D., Naudascher, E., 1979. Self-sustained oscillations of impinging free shear layer. Annual Review of Fluid Mechanics 11, 67–94.

Rossiter, J.E., 1964. Wind-tunnel experiments on the flow over rectangular cavities at subsonic and transonic speeds. Aeronautical Research Council Reports and Memoranda, No. 3438.

Sarohia, V., 1977. Experimental investigation of oscillations in flows over shallow cavities. AIAA Journal 15, 984–990.

Yao, H., Cooper, R.K., Raghunathan, S., 2004. Numerical simulation of incompressible laminar flow over three-dimensional rectangular cavities. ASME Journal of Fluids Engineering 126, 919–927.

Zhou, J., Adrian, R.J., Balachandar, S., Kendall, T.M., 1999. Mechanism for generating coherent packets of hairpin vortices in channel flow. Journal of Fluid Mechanics 387, 353–396.